



1 **A comprehensive study about the in-cloud processing of nitrate through**
2 **coupled measurements of individual cloud residuals and cloud water**

3

4 Guohua Zhang^{1,2,3}, Xiaodong Hu^{1,2,4}, Wei Sun^{1,2,4}, Yuxiang Yang^{1,2}, Ziyong Guo^{1,2,4}, Yuzhen Fu^{1,2}, Haichao

5 Wang⁵, Shengzhen Zhou⁵, Lei Li⁶, Mingjin Tang^{1,2,3}, Zongbo Shi⁷, Duohong Chen⁸, Xinhui Bi^{1,2,3,*}, Xinming

6 Wang^{1,2,3}

7

8 ¹ State Key Laboratory of Organic Geochemistry and Guangdong Provincial Key Laboratory
9 of Environmental Protection and Resources Utilization, Guangzhou Institute of
10 Geochemistry, Chinese Academy of Sciences (CAS), Guangzhou 510640, PR China

11 ² CAS Center for Excellence in Deep Earth Science, Guangzhou, 510640, China

12 ³ Guangdong-Hong Kong-Macao Joint Laboratory for Environmental Pollution and Control,
13 Guangzhou Institute of Geochemistry, CAS, Guangzhou 510640, PR China

14 ⁴ University of Chinese Academy of Sciences, Beijing 100049, PR China

15 ⁵ School of Atmospheric Sciences, Sun Yat-sen University, Guangzhou 519082, PR China

16 ⁶ Institute of Mass Spectrometer and Atmospheric Environment, Jinan University,
17 Guangzhou 510632, PR China

18 ⁷ School of Geography, Earth and Environmental Sciences, University of Birmingham,
19 Birmingham B15 2TT, U.K.

20 ⁸ State Environmental Protection Key Laboratory of Regional Air Quality Monitoring,
21 Guangdong Environmental Monitoring Center, Guangzhou 510308, PR China

22

23 Correspondence to: Xinhui Bi (bixh@gig.ac.cn)

24



25 **Abstract**

26 While the formation and evolution of nitrate in airborne particles are extensively
27 investigated, little is known about the processing of nitrate in clouds. Here we present a
28 detailed investigation on the in-cloud formation of nitrate, based on the size-resolved mixing
29 state of nitrate in the individual cloud residual and cloud-free particles obtained by single
30 particle mass spectrometry, and also the mass concentrations of nitrate in the cloud water
31 and PM_{2.5} at a mountain site (1690 m a.s.l.) in southern China. The results show a significant
32 enhancement of nitrate mass fraction and relative intensity of nitrate in cloud water and the
33 cloud residual particles, respectively, reflecting a critical role of in-cloud processing in the
34 formation of nitrate. We first exclude the gas phase scavenging of HNO₃ and the facilitated
35 activation of nitrate-containing particles as the major contribution for the enhanced nitrate,
36 according to the size distribution of nitrate in individual particles. Based on regression
37 analysis and theoretical calculations, we then reveal a critical role of in-cloud formation of
38 nitrate via N₂O₅ hydrolysis, even during the daytime, attributed to the diminished light in
39 clouds. Nitrate is highly related ($R^2 = \sim 0.6$) to the variation of [NO_x][O₃], temperature and
40 droplet surface area in clouds. Accounting for droplet surface area greatly enhances the
41 predictability of the observed nitrate compared with using [NO_x][O₃] and temperature. The
42 substantial contribution of N₂O₅ hydrolysis to nitrate in clouds during the daytime was
43 reproduced by a multiphase chemical box model. Assuming that the photolysis rate is 30%
44 of the default setting, the overall contribution of N₂O₅ hydrolysis pathway to nitrate
45 formation increases by ~20% in clouds. Given that N₂O₅ hydrolysis acts as a major sink of



46 NO_x in the atmosphere, further model updates would improve our understanding about the
47 processes contributing to nitrate production in cloud and the cycling of odd nitrogen.



48 **1. Introduction**

49 Aerosol nitrate is an increasingly important component of PM_{2.5}, in particular,
50 contributing to haze formation in China (Liu et al., 2020b; Xu et al., 2019; Zheng et al., 2020;
51 Fu et al., 2020; Guo et al., 2014; Tian et al., 2019; Wen et al., 2018; Lu et al., 2019). As a
52 key inorganic component in cloud water, nitrate can also modify microphysical properties
53 of cloud, influence aqueous-phase processes in droplets and affect ecosystem after wet
54 deposition (Schneider et al., 2017). Notably, aerosol nitrate is an important product in the
55 cycling of odd nitrogen (Chang et al., 2011; Zheng et al., 2020; Zhang et al., 2021; Huang et
56 al., 2018), playing significant roles in tropospheric ozone and OH production (Scharko et al.,
57 2014; Kaur and Anastasio, 2017; Ye et al., 2017a; Ye et al., 2017b), and contributing to net
58 aerosol composition and radiative forcing (Bauer et al., 2007; Hauglustaine et al., 2014; Xu
59 and Penner, 2012).

60 Aerosol nitrate originates from the oxidation of NO_x, which refers to gas phase
61 oxidation of NO₂ by the hydroxyl radical (OH) followed by condensation (daytime
62 chemistry) and the hydrolysis of N₂O₅ (nighttime chemistry) to nitrate in aqueous particles,
63 initiated by the oxidation of NO₂ by ozone (O₃) to produce the NO₃ radical (Seinfeld and
64 Pandis, 2006). In contrary to aerosol sulfate formation, which is dominated by aqueous phase
65 reactions, both gas phase oxidation and the hydrolysis of N₂O₅ represent the major processes
66 forming aerosol nitrate (Hayden et al., 2008; Sellegri et al., 2003; Fahey et al., 2005; Chen
67 et al., 2020; Xiao et al., 2020). Extensive studies have shown that the formation and evolution
68 of nitrate depend on various factors, such as the availability of ammonia (NH₃), temperature



69 (T), relative humidity (RH), and the presence of other ionic species in particulate phase
70 (Chen et al., 2018; Shi et al., 2019; Chen et al., 2020; Lin et al., 2021; Fan et al., 2021).

71 Comparatively, detailed observational investigations and the possible mechanisms
72 governing nitrate behavior upon in-cloud processes are scarce and poorly understood,
73 although it is well-known that clouds play an important role in the transport and
74 transformation of tropospheric pollutants (Li et al., 2020b; Ervens, 2015; McNeill, 2017).
75 Global model studies still disagree on the relative importance of in-cloud process
76 contributing to the production of HNO_3 . While most have neglected N_2O_5 and NO_3 uptake
77 in clouds (Alexander et al., 2009; Hauglustaine et al., 2014; Xu and Penner, 2012), there is
78 also research suggesting the significance of in-cloud process (Holmes et al., 2019). Likewise,
79 despite limited research, the role of clouds in nitrate formation from field observations
80 remains controversial. Drewnick et al. (2007) and Prabhakar et al. (2014) reported that the
81 relatively enhanced nitrate in clouds was associated with the composition of the activating
82 cloud condensation nuclei (CCN), rather than preferential scavenging of nitric acid (HNO_3)
83 in clouds. Differently, there are also studies highlighting the predominant role of nitric acid
84 partitioning in nitrate formation in clouds, in contrary to nucleation scavenging of sulfate
85 (Schneider et al., 2017; Hayden et al., 2008; Leaitch et al., 1988). Hayden et al. (2008) also
86 noted that potential contributions from gas-phase N_2O_5 cannot be ruled out. Therefore, more
87 detailed investigations are still required to integrate the role of cloud in the formation of
88 nitrate in the troposphere.

89 The aim of this study is to illustrate the in-cloud formation mechanisms of nitrate and



90 evaluate the relative contribution of each pathway to nitrate in cloud water for daytime and
91 nighttime. To this aim, the mixing state of individual cloud residual, interstitial and cloud-
92 free particles were measured in high-time resolution with a single particle aerosol mass
93 spectrometer (SPAMS). The combination of a counter flow virtual impactor (CVI) and
94 aerosol mass spectrometry (including SPAMS) allows for the high-time resolved
95 observations of size and chemical compositions of submicron cloud residual particles
96 (Boone et al., 2015; Hao et al., 2013; Zhang et al., 2017; Lin et al., 2017). In addition, cloud
97 water and PM_{2.5} samples were collected, and the chemical compositions were measured to
98 provide additional quantitative evidence.

99

100 **2. Experimental section**

101 **2.1 Aerosol and cloud measurements**

102 Aerosol and cloud measurements were performed at the Mt. Tianjing site (24°41'56"N,
103 112°53'56"E, 1690 m a.s.l.) in southern China, as described in detail by Lin et al. (2017),
104 during 9 May – 4 June 2018 and 13 November – 9 December 2020. Cloud events can be
105 distinguished by a sudden drop of visibility (to < ~1 km) and a sharp increase of relative
106 humidity (RH) to > 95%, as record by sensors equipped with a ground-based counterflow
107 virtual impactor (GCVI) (Model 1205, Brechtel Mfg. Inc., USA) (Lin et al., 2017). Overall,
108 nineteen cloud events (lasting more than six hours) were identified for 2018 spring and ten
109 for 2020 winter, as also marked in Fig. S1. The visibility was generally lower than 0.1 km
110 during the cloud events, versus as high as 80 km during the cloud-free periods. Besides a



111 relatively long cloud event throughout 9 – 12 May, the cloud events were typically observed
112 during nighttime for 2018 spring, associated with a prominently diurnal variation of RH and
113 visibility. The RH during the daytime ranged between 70-80%, and raised to > 95% during
114 nighttime. The duration of cloud events was in a range of 6-24 hours for 2020 winter. Air
115 masses from the southern continental and marine areas dominated over the 2018 spring and
116 2020 winter periods, with air masses from western continental areas unique for the 2020
117 winter (Fig. S2), obtained by HYSPLIT 4.9 (<http://ready.arl.noaa.gov/HYSPLIT.php>)
118 (Draxler and Rolph, 2012).

119 An incorporation of counterflow virtual impactor (CVI) or GCVI allows the separation
120 of interstitial gases and aerosols from cloud droplets that are evaporated to obtain the cloud
121 residual particles (Bi et al., 2016; Roth et al., 2016; Pratt et al., 2009). Briefly, the GCVI was
122 applied to collect the cloud droplets with predefined size (7.5-8.5 μm in the present study),
123 with the cloud residual particles as output after dried in the evaporation chamber (with an air
124 flow temperature at 40 °C) (Shingler et al., 2012). The influence of cloud-free air can be
125 negligible as the number concentration of GCVI output particles was measured to be $\sim 1 \text{ cm}^{-3}$
126 3 , but at a magnitude of $\sim 10^3 \text{ cm}^{-3}$ in the cloud-free air. In the present study, the average
127 number concentration of the cloud residual particles sampled during the cloud events was at
128 a level of $\sim 100 \text{ cm}^{-3}$. In addition, a $\text{PM}_{2.5}$ inlet was used to deliver cloud interstitial particles
129 during cloud events or cloud-free particles.

130

131 **2.2 SPAMS measurements and data processing**



132 A SPAMS (Hexin Analytical Instrument Co., Ltd., Guangzhou, China), an Aethalometer
133 (AE-33, Magee Scientific Inc.), and a scanning mobility particle sizer (SMPS; MSP
134 Cooperation) were deployed to characterize the physical and chemical properties of the
135 sampled particles. The instruments were connected downstream the GCVI or PM_{2.5} inlets.
136 Cloud residual and cloud interstitial particles were alternately sampled with an interval of
137 ~1 h during some randomly selected cloud events. During the cloud free period, these
138 instruments were connected to the PM_{2.5} inlet in order to measure the cloud-free particles.
139 In the present study, aerosol surface area (SA) for cloud-free particles were directly
140 calculated from the size distribution data obtained from SMPS, whereas it can only be
141 estimated based on the same data for the cloud residues assuming a mean droplet size at 7
142 μm . We recognize the possible uncertainty, but the estimated SA should correlate with real
143 values and thus would not lead to ambiguous conclusions.

144 The vacuum aerodynamic diameter (d_{va}) and mass spectral information for individual
145 particles were measured by the SPAMS (Li et al., 2011). A brief description on the
146 performance of the SPAMS can also be found in the Supplement. Over the sampling period
147 for the 2018 spring and 2020 winter periods, a respective ~20, 000, 000 particles with mass
148 spectral information were analyzed, using the FATEs toolkit based on Matlab (The
149 MathWorks, Inc.) (Sultana et al., 2017). The particles were classified by an adaptive
150 resonance theory-based neural network algorithm (Song et al., 1999), with the inputs of ion
151 peak intensities. Seven types with distinct mass spectral characteristics (Fig. S3), accounting
152 for > 95% of all the detected particles, were obtained for further analysis. The presence of



153 nitrate can be identified with ion peaks (defined as five times the noise signal) at m/z -62
154 $[\text{NO}_3]^-$ or m/z -46 $[\text{NO}_2]^-$. Approximate 70-80% of all the detected particles in the size range
155 of 100-2000 nm contained nitrate ion signals for our measurements. Defined as fractional
156 peak area of each m/z relative to the sum of peak areas in a mass spectrum, relative peak
157 area (RPA) is applied to represent the relative amount of a species within a particle (Jeong
158 et al., 2011; Healy et al., 2013).

159

160 **2.3 Cloud water/ $\text{PM}_{2.5}$ collection and chemical analysis**

161 A Caltech Active Strand Cloud Water Collector (CASCC2) was applied to collect cloud
162 water (with droplet size $> 3.5 \mu\text{m}$). The average cloud liquid water content (LWC) for each
163 sampling period can be derived from $\text{LWC} = \Delta m / (\Delta t \times \eta \times Q)$, based on each sample mass
164 (Δm), duration time (Δt), flow rate ($Q = 5.8 \text{ m}^3 \text{ min}^{-1}$), and collection efficiency ($\eta = 86\%$).

165 A total of 58 / 53 cloud water samples were collected over the nineteen / ten cloud events
166 for 2018 spring and 2020 winter periods, respectively, with the durations ranging between 2
167 and 10 hours. The pH for collected samples were immediately measured using a pH meter
168 (Mettler Toledo, Switzerland) after filtered through a $0.22 \mu\text{m}$ filter, followed by kept at -
169 $20 \text{ }^\circ\text{C}$ until the analysis.

170 $\text{PM}_{2.5}$ samples were collected on quartz filters using a $\text{PM}_{2.5}$ sampler (PM-PUF-300,
171 Mingye Instruments, China) at a flow rate of 300 L min^{-1} . The filter were pre-conditioned in
172 $450 \text{ }^\circ\text{C}$ for 6 hours to eliminate the potential influence of organics. A total of 20 / 36 $\text{PM}_{2.5}$
173 samples were collected for the 2018 spring and 2020 winter periods, respectively. The



174 samples were kept at $-20\text{ }^{\circ}\text{C}$ immediately until further analysis. These samples are
175 representative for the cloud-free particles or cloud interstitial particles during cloud events.

176 Cloud water and $\text{PM}_{2.5}$ samples were analyzed with ion chromatograph (Metrohm 883
177 IC plus, Switzerland) for water soluble inorganic ions (Na^+ , NH_4^+ , K^+ , Ca^{2+} , Mg^{2+} , Cl^- , NO_3^- ,
178 and SO_4^{2-}) and total organic carbon analyzer (Vario, Elementar, Germany for 2018 samples
179 and TOC-V, Shimadzu, Japan for 2020 samples) for water soluble organic carbon (WSOC).
180 The overall uncertainty for the concentration of each species is calculated to be $< 15\%$ based
181 on parallel analyses. The nitrate mass fractions in cloud water and $\text{PM}_{2.5}$ were calculated by
182 dividing the nitrate concentration by the sum of the measured water-soluble inorganic ions
183 and water-soluble organic matter (estimated by $1.6 \cdot \text{WSOC}$).

184

185 **2.4 Box modeling of nitrate formation in cloud**

186 A multiphase chemical box model (RACM-CAPRAM) was used to simulate the
187 production of nitrate in wet aerosols and cloud droplets. It couples the regional atmospheric
188 chemistry mechanism version 2 (RACM2; including 363 chemical reactions) and the
189 chemical aqueous-phase radical mechanism version 2.4 (CAPRAM2.4; including 438
190 chemical reactions) to account for gas- and aqueous-phase atmospheric chemistry (Ervens
191 et al., 2003). As similarly performed in previous studies (Pathak et al., 2009; Wen et al.,
192 2018), three major pathways for nitrate formation are considered: (1) The oxidation of NO_2
193 by the OH radical produces HNO_3 and partitioning of gaseous HNO_3 into the aqueous phase;
194 (2) The hydrolysis reactions of N_2O_5 ; and (3) The aqueous-phase reactions of NO_3 radicals.



195 The average concentration of NO₂ (~25 ppb) and O₃ (~100 ppb) for gas-phase precursors
196 and LWC (0.1 g m⁻³) for cloud droplets, obtained from the in-situ measurements, were taken
197 as representative parameters for the atmosphere condition at Mt. Tianjing, and used as initial
198 conditions for model simulation. The detailed initial conditions for the model are listed in
199 the SI Table S1. Several comparisons through varying the LWC and photolysis rate were
200 considered in order to investigate the role of LWC and photolysis on the formation of nitrate
201 in the cloud. It is also noted that only LWC and photolysis rate were reset in our scenario,
202 with other factors (e.g., initial droplet composition, SO₂) kept as default setting in the model
203 setup.

204

205 **3. Results and discussion**

206 **3.1. Enhanced in-cloud production of nitrate**

207 Figure 1 shows the statistical results of the nitrate mass fractions in cloud water and
208 PM_{2.5} and the hourly average relative intensity of nitrate (represented by the RPA) in the
209 cloud-free, cloud residual, and cloud interstitial particles. The results clearly indicate the
210 enhancement of nitrate in clouds. It can be seen that the mass fraction of nitrate in cloud
211 water (~20% on average) is obviously higher than those in PM_{2.5} (< 15% on average) during
212 the cloud-free periods and cloud events, for both the 2018 spring and 2020 winter periods.
213 Consistently, the relative intensity of nitrate was substantially enhanced in the cloud
214 interstitial particles and particularly cloud residues, relative to the cloud-free particles. The
215 influence of air mass on the enhanced nitrate can be ruled out for the 2018 spring period, as



216 they similarly originated from southern areas over the whole campaign period (Fig. S2).
217 While the air masses originated from different regions during the 2020 winter period, they
218 did not show the difference between the cloud-free periods and cloud events, with the
219 shifting of air masses and/or wind direction after 27 Nov (Figs. S1 and S2). Thus, the
220 influence of air mass on the enhanced nitrate in 2020 winter should also be limited.

221 There are several pathways that might contribute to the enhanced nitrate in cloud
222 droplets, including (1) the scavenging of gas-phase HNO_3 , (2) the preferential activation of
223 nitrate-rich particles, and (3) in-cloud aqueous production of nitrate via reaction of NO_3
224 radicals or hydrolysis of N_2O_5 . The mechanism via the dissolution of NO_2 and its aqueous
225 phase oxidation is relatively slow and unlikely to be a significant source of cloud water
226 nitrate (Seinfeld and Pandis, 2006).

227 We first exclude the scavenging of gas-phase HNO_3 as a major pathway through the
228 analysis of size distribution of nitrate RPA and RPA ratio (nitrate / sulfate), although all the
229 gas phase HNO_3 could be efficiently scavenged and present in the aqueous phase in a typical
230 cloud with $\text{LWC} > 0.1 \text{ g m}^{-3}$ (Seinfeld and Pandis, 2006). As can be seen in Fig. 2, the RPA
231 of nitrate and RPA ratios of nitrate to sulfate distributes relatively stable over the measured
232 size range, which suggests that the gas phase scavenging of HNO_3 is not the dominant
233 pathway in the present conditions. This is because gas-phase mass transfer would lead to
234 enhanced nitrate in the smaller droplets with higher total surface area (Drewnick et al., 2007).
235 As also discussed in the following section, the formation of HNO_3 would be certainly
236 suppressed by the presence of cloud.



237 We also indicate that the contribution of preferential activation of the nitrate-rich
238 particles should be limited since such a process would lead to the depletion of nitrate in the
239 cloud interstitial particles relative to the cloud-free particles. But this is not the case, as the
240 RPA of nitrate and RPA ratios of nitrate to sulfate in the cloud interstitial particles are
241 considerably higher than those in the cloud-free particles (Fig. 2). Both the enhanced nitrate
242 in the cloud residual and interstitial particles suggest the in-cloud formation of nitrate,
243 although the variation of nitrate RPA cannot provide a quantitative view. The enhancement
244 of nitrate in the cloud interstitial particles may also indicate that in-cloud condition facilitates
245 the formation of nitrate even in the inactivated particles. Similar results have also been
246 observed in our previous study for oxalate (Zhang et al., 2017). Consistently, the formation
247 of nitrate in the cloud interstitial particles also grows their size towards the larger mode,
248 compared with the cloud-free particles (Fig. S4).

249

250 **3.2. In-cloud nitrate formation**

251 A theoretical estimation of nitrate production for 2020 winter is performed based on the
252 well-established kinetic characteristic of reactions between NO_2 and O_3 and uptake of N_2O_5
253 onto aerosol/droplet surfaces that formed HNO_3 (SI text S1), corresponding to the nighttime
254 chemistry. It is reasonable since the heterogeneous hydrolysis of N_2O_5 within aerosol
255 particles, fog, or cloud droplets has been shown to be much faster than homogeneous
256 hydrolysis under typical tropospheric conditions (Chang et al., 2011; Wang et al., 2017).
257 Through integrating the rate equations, as listed in SI text S1, the solution for aqueous phase



258 production of HNO₃ can be obtained (Seinfeld and Pandis, 2006):

$$259 \quad [\text{HNO}_3] = \frac{[\text{NO}_x]}{2} \left\{ 1 + \frac{1}{\tau_{\text{NO}_x} - \tau_{\text{N}_2\text{O}_5}} \left[\tau_{\text{N}_2\text{O}_5} \exp\left(-\frac{t}{\tau_{\text{N}_2\text{O}_5}}\right) - \tau_{\text{NO}_x} \exp\left(-\frac{t}{\tau_{\text{NO}_x}}\right) \right] \right\}$$

260 Thus, the conversion of NO_x to HNO₃ through the hydrolysis of N₂O₅ depends on the
261 two lifetimes τ_{NO_x} and $\tau_{\text{N}_2\text{O}_5}$, as defined by the reaction kinetics (SI text S1). The key
262 reaction that formed aqueous phase nitrate is related to the effective reaction of N₂O₅ on the
263 surface of wet aerosol or droplets (Holmes et al., 2019), and therefore, depends on the
264 concentration of NO₂ and O₃ ([NO₂][O₃]), the available aerosol and droplet SA, and
265 temperature. Besides the reaction kinetics, temperature could also have influence on the
266 hydrolysis of N₂O₅ (Chen et al., 2018; Chang et al., 2011).

267 As shown in Fig. 3, the theoretically calculated in-cloud nitrate production assuming a
268 typical uptake coefficient of N₂O₅ $\gamma = 0.06$ (Seinfeld and Pandis, 2006) could well match the
269 measured nitrate concentrations well (with $R^2 = 0.38$ and 0.60 at $p < 0.01$ for daytime and
270 nighttime, respectively), varying in a wide range of $\sim 1 \text{ mg L}^{-1}$ to $\sim 60 \text{ mg L}^{-1}$ for 2020 winter.
271 The correlation coefficients are obviously higher than those predicted using only [NO_x][O₃]
272 (with $R^2 = 0$ and 0.54 for daytime and nighttime, respectively). This is consistent with
273 previous results that the nighttime production of N₂O₅ and HNO₃ would be proportional to
274 the concentration of NO₂ and O₃ ([NO₂][O₃]) when assuming N₂O₅ and the NO₃ radical are
275 both in steady state considering their short lifetimes (Li et al., 2018; Wang et al., 2017). The
276 result also highlights the significance of SA in the in-cloud N₂O₅ hydrolysis in the build-up
277 of nitrate through in-cloud processing, even during the daytime. A further comparison of
278 [NO_x][O₃] and SA for the cloud events and cloud free periods, as shown in Fig. S5, also



279 supports the above discussion that the higher fraction of nitrate cannot be well explained by
280 the variations of $[\text{NO}_x][\text{O}_3]$, but rather by the enhanced SA due to the presence of droplets
281 (Fig. S5b), which is > 5 times on average that for aerosol particles during cloud-free periods.
282 In the present study, the average LWC of cloud droplets is at a level of $\sim 10^5 \mu\text{g m}^{-3}$, 3-4
283 magnitude higher than those for urban haze conditions. As previously reported, high aerosol
284 LWC (campaign average at $\sim 50 \mu\text{g m}^{-3}$) induced fast heterogeneous uptake coefficient of
285 N_2O_5 is prevalent in urban haze (Chang et al., 2011; Wang et al., 2017), and results in
286 enhanced nitrate in highly humid condition (Neuman et al., 2003; Wang et al., 2009; Pathak
287 et al., 2009).

288 The theoretical estimate indicates that the hydrolysis of N_2O_5 may substantially
289 contribute to the in-cloud production of nitrate even during the daytime, consistent with the
290 observation results as discussed in Section 3.1. It is also noted that theoretically predicted
291 nitrate production from the hydrolysis of N_2O_5 represents $\sim 5\text{-}10\%$ of the measured nitrate
292 (Fig. 3) based on our assumption. It explains $\sim 1\text{-}3\%$ increase in the nitrate mass fraction in
293 clouds, whereas the in-cloud processing contributed to $> 5\%$ increase (Fig. 1). One reason is
294 that the assumed $\gamma = 0.06$ might not be representative for N_2O_5 uptake in cloud droplets,
295 since the previously reported γ varies in a wide range, depending on various factors (e.g.,
296 droplet compositions, pH, temperature) (Bertram and Thornton, 2009; Holmes et al., 2019;
297 Burkholder et al., 2015). Some higher γ (0.2-0.4) was also observed for deliquescent sodium
298 sulfate particles (Burkholder et al., 2015). Another reason is that the SA estimated by the
299 size distribution data of cloud residues obtained by the GCVI-SMPS only represents part ($<$



300 50%) of the cloud droplets, as GCVI was set to collect droplets larger than 7.0 μm in the
301 present study.

302 Furthermore, a simplified regression and a random forest analysis are also performed
303 for the high-time resolved RPAs of nitrate obtained by the SPAMS, with $[\text{NO}_x][\text{O}_3]$, SA,
304 and temperature as inputs, separated for the cloud RES and cloud-free particles, as detailed
305 in SI text S2. Note that the concentration of NO_x is used here to represent that of NO_2 , since
306 most of NO data were not available for the 2018 spring. The effect should be limited since
307 NO could be negligible when the air masses are dominantly attributed to long range transport,
308 which could also be supported by the data (NO , $\sim 0.1 \mu\text{g m}^{-3}$, $< 2\%$ of NO_2 concentration) in
309 2020 winter. As expected, the nitrate RPA in the cloud residual particles is highly correlated
310 to the predicted ones ($R^2 = 0.75$ and 0.71 with $p < 0.01$ for the daytime and nighttime,
311 respectively), even during the daytime (**Fig. 4**). An inclusion of temperature and SA in the
312 model substantially improves the correlation coefficient R^2 , which is originally 0.16 and 0.31
313 between the nitrate RPA and $[\text{NO}_x][\text{O}_3]$ for the daytime and nighttime, respectively.
314 Similarly, the correlation coefficients ($R^2 = 0.45$ and 0.66 for daytime and nighttime,
315 respectively) are lower for 2018 spring than 2020 winter, without the availability of SA data.
316 The results are generally consistent with those obtained from random forest analysis, as
317 shown in Fig. S6. Without the input of SA, $[\text{NO}_x][\text{O}_3]$ and temperature only explains 52-61%
318 of the observed nitrate RPA for cloud residual particles in 2018 spring, compared with 72-
319 80% in 2020 winter. Compared with the cloud residual particles, the predictions for the
320 nitrate RPA in the cloud-free particles are of lower coefficients. Such difference between the



321 cloud residual and cloud-free particles also reflects the critical role of SA in the hydrolysis
322 of N_2O_5 in cloud droplets.

323

324 **3.3. Relative importance of N_2O_5 hydrolysis pathway to nitrate in clouds**

325 The relative contribution of nitrate formation in the cloud droplets and cloud-free
326 particles is also assessed using the CAPRAM model, as shown in Fig. 5. The relative
327 contribution difference between the cloud droplets and cloud-free particles is primarily
328 attributed to the different LWC setting, which is tightly linked to the cloud droplets' SA.
329 Furthermore, the comparison between cloud scenarios with different LWC setting (0.05 g m^{-3}
330 versus 0.15 g m^{-3}) also shows an enhanced contribution of N_2O_5 hydrolysis to nitrate with
331 increasing LWC.

332 Nitrate is known to form predominantly by the hydrolysis of N_2O_5 (> 80%) for both the
333 cloud droplets and cloud-free particles for the nighttime. However, both Fig. 3 and Fig. 4
334 indicate the potential importance of the heterogeneous N_2O_5 hydrolysis to nitrate formation
335 during the daytime. This is likely attributed to the substantial attenuation of the incident solar
336 radiation by clouds, in which the visibility was as low as < 0.1 km over this study. Previous
337 studies have also indicated the effect of clouds in the vertical redistribution of the
338 photochemical activity (Liu et al., 2006; Hall et al., 2018). Most comparatively, Brown et al.
339 (2016) observed a discrepancy between the modelled and observed N_2O_5 during a daytime
340 fog episode in Hong Kong, and attributed to the uptake of N_2O_5 to fog droplets. Their
341 calculation infers that daytime production of soluble nitrate via N_2O_5 can be substantially



342 faster than photochemical conversion through OH+NO₂ in the polluted fog episodes (Brown
343 et al., 2016).

344 The model results in Fig. 5 with the consideration of photolysis rate are, to some extent,
345 consistent with our observations. The overall contribution of N₂O₅ hydrolysis pathways
346 increases by ~20% (from ~50-60% to ~70-80%) when the photolysis rate is reduced to 30%
347 of the default setting. For daytime only, the contribution of this pathway also increases from
348 nearly 0 to ~20% during the noon hours and ~40% for the morning hours. A similar model
349 study also indicates that N₂O₅ hydrolysis contributed to 30% of daytime nitrate formation at
350 Mt. Tai (Zhu et al., 2020). Attributed to the substantial attenuation of incident solar radiation
351 by clouds and high loading of PM_{2.5}, the daytime N₂O₅ hydrolysis has also been observed to
352 be an important formation pathway for nitrate in the haze episodes in Xi'an (China), and the
353 contribution increases from 8.2% to 20.5% of the total nitrate over 14:00–16:00 by model
354 simulation (Wu et al., 2021). Similarly, Liu et al. (2020a) showed that the daytime N₂O₅
355 hydrolysis contributed to ~10% of nitrate in the north China plain in winter. Note that
356 biogenic volatile organic compounds could also have a potentially important impact on
357 nitrate formation through affecting the oxidant concentrations (Aksoyoglu et al., 2017;
358 Zhang et al., 2019), yet remains to be quantified. However, the modelling results could still
359 indicate the role of cloud in the hydrolysis of N₂O₅, which contributes to the enhanced nitrate.
360

361 4. Conclusions and atmospheric implications

362 The presented results provide direct evidence that in-cloud aqueous processing, in



363 particular, the hydrolysis of N_2O_5 significantly contributes to the enhanced nitrate in cloud
364 residues. We highlight that the hydrolysis of N_2O_5 serves as the critical route for the in-cloud
365 formation of nitrate, even during the daytime. The dependence of in-cloud nitrate formation
366 on the cloud droplets' SA extends the observation fact that higher RH facilitates the formation
367 of nitrate in wet aerosols (Neuman et al., 2003; Wang et al., 2009; Pathak et al., 2009). Given
368 that N_2O_5 hydrolysis acts as a major sink of NO_x in the atmosphere (Yan et al., 2019), further
369 model updates may improve our understanding of the relative importance of nitrate-
370 production pathways (Chan et al., 2021; Alexander et al., 2020). In addition, significant
371 hydrolysis of N_2O_5 in cloud may also pose substantial effect on the tropospheric ozone
372 budget (Riemer et al., 2003; Voulgarakis et al., 2009; Strode et al., 2017).

373 As sulfate is reduced in the future through emission controls (Li et al., 2020a; Chu et al.,
374 2020), higher nitrate fraction is expected in cloud (Herckes et al., 2007; Herckes et al., 2015).
375 However, the limited dependence of nitrate formation on the $[\text{NO}_x][\text{O}_3]$ in the cloud suggest
376 a possibility that controlling NO_x and O_3 might be offset in the cloudy regions. Given the
377 significance of both emission and deposition on the variations of nitrate (Zhai et al., 2021)
378 and the contribution of the transported NO_x and O_3 to the notable effect and complex process
379 of cross-regional nitrate formation (Qu et al., 2021), knowledge of the in-cloud formation of
380 nitrate would also benefit $\text{PM}_{2.5}$ pollution control target over a larger scale.

381 Furthermore, our results indicate that in-cloud formed nitrate remains in particulate
382 phase after cloud evaporation (Fig. S7), changing the mixing state of individual particles.
383 Enhanced aerosol nitrate is expected to have higher hygroscopicity after cloud evaporation



384 (Sun et al., 2018; Hodas et al., 2014), and therefore, an increase of the particles' ability to act
385 as cloud condensation nuclei after their cloud passage (Roth et al., 2016). This is different
386 from that observed in California coast that the nitrate-to-sulfate mass ratio decreases rapidly
387 with cloud height, due to the volatilization during drop evaporation pushes NO_3 to the gas
388 phase (Prabhakar et al., 2014). In addition, vertical turbulent mixing of the residual aerosols
389 from evaporating cloud droplets may contribute to the nitrate aerosol loading during the
390 daytime at the ground level (Tao et al., 2018).



391 **Competing interests**

392 The authors declare that they have no conflict of interest.

393 **Data availability**

394 All the data can be obtained by contacting the corresponding author.

395 **Author contribution**

396 GHZ and XHB designed the research (with input from LL, MT, and XW), analyzed the
397 data (with input from XDH and WS), and wrote the paper. YXY, ZYG, and YZF performed the
398 field measurements and analyzed the collected samples. DHC, HCW, SZZ, and ZBS provided
399 constructive comments. All authors contributed to the refinement of the manuscript.

400 **Acknowledgement**

401 Thanks to Prof. Likun Xue (Shandong University) and Dr. Liang Wen (Leibniz Institute for
402 Tropospheric Research) for their support of the box modeling of nitrate formation in cloud.

403 **Financial support**

404 This work was funded by the Natural Science Foundation of Guangdong Province
405 (2019B151502022), National Natural Science Foundation of China (42077322, 41775124, and
406 41877307), Youth Innovation Promotion Association CAS (2021354), and Guangdong
407 Foundation for Program of Science and Technology Research (2020B1212060053).



408 **References**

- 409 Aksoyoglu, S., Ciarelli, G., El-Haddad, I., Baltensperger, U., and Prevot, A. S. H.: Secondary
410 inorganic aerosols in Europe: sources and the significant influence of biogenic VOC emissions,
411 especially on ammonium nitrate, *Atmos. Chem. Phys.*, 17, 7757-7773, doi:10.5194/acp-17-
412 7757-2017, 2017.
- 413 Alexander, B., Hastings, M. G., Allman, D. J., Dachs, J., Thornton, J. A., and Kunasek, S. A.:
414 Quantifying atmospheric nitrate formation pathways based on a global model of the oxygen
415 isotopic composition ($\Delta^{17}\text{O}$) of atmospheric nitrate, *Atmos. Chem. Phys.*, 9, 5043-5056,
416 doi:10.5194/acp-9-5043-2009, 2009.
- 417 Alexander, B., Sherwen, T., Holmes, C. D., Fisher, J. A., Chen, Q., Evans, M. J., and Kasibhatla,
418 P.: Global inorganic nitrate production mechanisms: comparison of a global model with nitrate
419 isotope observations, *Atmos. Chem. Phys.*, 20, 3859-3877, doi:10.5194/acp-20-3859-2020,
420 2020.
- 421 Bauer, S. E., Koch, D., Unger, N., Metzger, S. M., Shindell, D. T., and Streets, D. G.: Nitrate
422 aerosols today and in 2030: a global simulation including aerosols and tropospheric ozone,
423 *Atmos. Chem. Phys.*, 7, 5043-5059, doi:10.5194/acp-7-5043-2007, 2007.
- 424 Bertram, T. H., and Thornton, J. A.: Toward a general parameterization of N_2O_5 reactivity on
425 aqueous particles: the competing effects of particle liquid water, nitrate and chloride, *Atmos.*
426 *Chem. Phys.*, 9, 8351-8363, doi:10.5194/acp-9-8351-2009, 2009.
- 427 Bi, X. H., Lin, Q. H., Peng, L., Zhang, G. H., Wang, X. M., Brechtel, F. J., Chen, D. H., Li, M.,
428 Peng, P. A., Sheng, G. Y., and Zhou, Z.: In situ detection of the chemistry of individual fog
429 droplet residues in the Pearl River Delta region, China, *J. Geophys. Res.-Atmos.*, 121, 9105-
430 9116, doi:10.1002/2016JD024886, 2016.
- 431 Boone, E. J., Laskin, A., Laskin, J., Wirth, C., Shepson, P. B., Stirm, B. H., and Pratt, K. A.:
432 Aqueous Processing of Atmospheric Organic Particles in Cloud Water Collected via Aircraft
433 Sampling, *Environ. Sci. Technol.*, 49, 8523-8530, doi:10.1021/acs.est.5b01639, 2015.
- 434 Brown, S. S., Dube, W. P., Tham, Y. J., Zha, Q. Z., Xue, L. K., Poon, S., Wang, Z., Blake, D. R.,
435 Tsui, W., Parrish, D. D., and Wang, T.: Nighttime chemistry at a high altitude site above Hong



-
- 436 Kong, J. *Geophys. Res.-Atmos.*, 121, 2457-2475, doi:10.1002/2015JD024566, 2016.
- 437 Burkholder, J. B., Sander, S. P., Abbatt, J., Barker, J. R., Huie, R. E., Kolb, C. E., Kurylo, M. J.,
438 Orkin, V. L., Wilmouth, D. M., and Wine, P. H.: Chemical kinetics and photochemical data for
439 use in atmospheric studies C, edited by: Evaluation No. 18, J. P.-. National Aeronautics and
440 Space Administration, <http://jpldataeval.jpl.nasa.gov> (last access: 10 May 2022), 2015.
- 441 Chan, Y.-C., Evans, M. J., He, P., Holmes, C. D., Jaegle, L., Kasibhatla, P., Liu, X.-Y., Sherwen,
442 T., Thornton, J. A., Wang, X., Xie, Z., Zhai, S., and Alexander, B.: Heterogeneous Nitrate
443 Production Mechanisms in Intense Haze Events in the North China Plain, *J. Geophys. Res.-*
444 *Atmos.*, 126, doi:10.1029/2021jd034688, 2021.
- 445 Chang, W. L., Bhave, P. V., Brown, S. S., Riemer, N., Stutz, J., and Dabdub, D.: Heterogeneous
446 Atmospheric Chemistry, Ambient Measurements, and Model Calculations of N₂O₅: A Review,
447 *Aerosol Sci. Tech.*, 45, 665-695, doi:10.1080/02786826.2010.551672, 2011.
- 448 Chen, X., Wang, H., Lu, K., Li, C., Zhai, T., Tan, Z., Ma, X., Yang, X., Liu, Y., Chen, S., Dong,
449 H., Li, X., Wu, Z., Hu, M., Zeng, L., and Zhang, Y.: Field Determination of Nitrate Formation
450 Pathway in Winter Beijing, *Environ. Sci. Technol.*, 54, 9243-9253, doi:10.1021/acs.est.0c00972,
451 2020.
- 452 Chen, Y., Wolke, R., Ran, L., Birmili, W., Spindler, G., Schroder, W., Su, H., Cheng, Y. F., Tegen,
453 I., and Wiedensohler, A.: A parameterization of the heterogeneous hydrolysis of N₂O₅ for mass-
454 based aerosol models: improvement of particulate nitrate prediction, *Atmos. Chem. Phys.*, 18,
455 673-689, doi:10.5194/acp-18-673-2018, 2018.
- 456 Chu, B., Ma, Q., Liu, J., Ma, J., Zhang, P., Chen, T., Feng, Q., Wang, C., Yang, N., Ma, H., Ma,
457 J., Russell, A. G., and He, H.: Air Pollutant Correlations in China: Secondary Air Pollutant
458 Responses to NO_x and SO₂ Control, *Environ. Sci. Tech. Lett.*, 7, 695-700,
459 doi:10.1021/acs.estlett.0c00403, 2020.
- 460 Draxler, R. R., and Rolph, G. D.: HYSPLIT (HYbrid Single-Particle Lagrangian Integrated
461 Trajectory) Model access via NOAA ARL READY Website
462 (<http://ready.arl.noaa.gov/HYSPLIT.php>), NOAA Air Resources Laboratory, MD, Silver Spring,
463 2012.
- 464 Drewnick, F., Schneider, J., Hings, S. S., Hock, N., Noone, K., Targino, A., Weimer, S., and



-
- 465 Borrmann, S.: Measurement of ambient, interstitial, and residual aerosol particles on a
466 mountaintop site in central Sweden using an aerosol mass spectrometer and a CVI, *J. Atmos.*
467 *Chem.*, 56, 1-20, doi:10.1007/s10874-006-9036-8, 2007.
- 468 Ervens, B., George, C., Williams, J. E., Buxton, G. V., Salmon, G. A., Bydder, M., Wilkinson,
469 F., Dentener, F., Mirabel, P., Wolke, R., and Herrmann, H.: CAPRAM 2.4 (MODAC
470 mechanism): An extended and condensed tropospheric aqueous phase mechanism and its
471 application, *J. Geophys. Res.-Atmos.*, 108, doi:10.1029/2002jd002202, 2003.
- 472 Ervens, B.: Modeling the Processing of Aerosol and Trace Gases in Clouds and Fogs, *Chem.*
473 *Rev.*, 115, 4157-4198, doi:10.1021/cr5005887, 2015.
- 474 Fahey, K. M., Pandis, S. N., Collett, J. L., and Herckes, P.: The influence of size-dependent
475 droplet composition on pollutant processing by fogs, *Atmos. Environ.*, 39, 4561-4574,
476 doi:10.1016/j.atmosenv.2005.04.006, 2005.
- 477 Fan, M. Y., Zhang, Y. L., Lin, Y. C., Hong, Y., Zhao, Z. Y., Xie, F., Du, W., Cao, F., Sun, Y., and
478 Fu, P.: Important Role of NO₃ Radical to Nitrate Formation Aloft in Urban Beijing: Insights
479 from Triple Oxygen Isotopes Measured at the Tower, *Environ. Sci. Technol.*,
480 doi:10.1021/acs.est.1c02843, 2021.
- 481 Fu, X., Wang, T., Gao, J., Wang, P., Liu, Y., Wang, S., Zhao, B., and Xue, L.: Persistent Heavy
482 Winter Nitrate Pollution Driven by Increased Photochemical Oxidants in Northern China,
483 *Environ. Sci. Technol.*, 54, 3881-3889, doi:10.1021/acs.est.9b07248, 2020.
- 484 Guo, S., Hu, M., Zamora, M. L., Peng, J., Shang, D., Zheng, J., Du, Z., Wu, Z., Shao, M., Zeng,
485 L., Molina, M. J., and Zhang, R.: Elucidating severe urban haze formation in China, *Proc. Natl.*
486 *Acad. Sci. USA*, 111, 17373, doi:10.1073/pnas.1419604111, 2014.
- 487 Hall, S. R., Ullmann, K., Prather, M. J., Flynn, C. M., Murray, L. T., Fiore, A. M., Correa, G.,
488 Strode, S. A., Steenrod, S. D., Lamarque, J.-F., Guth, J., Josse, B., Flemming, J., Huijnen, V.,
489 Abraham, N. L., and Archibald, A. T.: Cloud impacts on photochemistry: building a climatology
490 of photolysis rates from the Atmospheric Tomography mission, *Atmos. Chem. Phys.*, 18, 16809-
491 16828, doi:10.5194/acp-18-16809-2018, 2018.
- 492 Hao, L., Romakkaniemi, S., Kortelainen, A., Jaatinen, A., Portin, H., Miettinen, P., Komppula,
493 M., Leskinen, A., Virtanen, A., Smith, J. N., Sueper, D., Worsnop, D. R., Lehtinen, K. E. J., and



-
- 494 Laaksonen, A.: Aerosol Chemical Composition in Cloud Events by High Resolution Time-of-
495 Flight Aerosol Mass Spectrometry, *Environ. Sci. Technol.*, 47, 2645-2653,
496 doi:10.1021/es302889w, 2013.
- 497 Hauglustaine, D. A., Balkanski, Y., and Schulz, M.: A global model simulation of present and
498 future nitrate aerosols and their direct radiative forcing of climate, *Atmos. Chem. Phys.*, 14,
499 11031-11063, doi:10.5194/acp-14-11031-2014, 2014.
- 500 Hayden, K. L., Macdonald, A. M., Gong, W., Toom-Saunty, D., Anlauf, K. G., Leithead, A., Li,
501 S. M., Leaitch, W. R., and Noone, K.: Cloud processing of nitrate, *J. Geophys. Res.-Atmos.*,
502 113, 1-18, doi:10.1029/2007jd009732, 2008.
- 503 Healy, R. M., Sciare, J., Poulain, L., Crippa, M., Wiedensohler, A., Prevot, A. S. H.,
504 Baltensperger, U., Sarda-Estevé, R., McGuire, M. L., Jeong, C. H., McGillicuddy, E., O'Connor,
505 I. P., Sodeau, J. R., Evans, G. J., and Wenger, J. C.: Quantitative determination of carbonaceous
506 particle mixing state in Paris using single-particle mass spectrometer and aerosol mass
507 spectrometer measurements, *Atmos. Chem. Phys.*, 13, 9479-9496, doi:10.5194/acp-13-9479-
508 2013, 2013.
- 509 Herckes, P., Chang, H., Lee, T., and Collett, J. L.: Air pollution processing by radiation fogs,
510 *Water Air Soil Pollut.*, 181, 65-75, doi:10.1007/s11270-006-9276-x, 2007.
- 511 Herckes, P., Marcotte, A. R., Wang, Y., and Collett, J. L.: Fog composition in the Central Valley
512 of California over three decades, *Atmos. Res.*, 151, 20-30, doi:10.1016/j.atmosres.2014.01.025,
513 2015.
- 514 Hodas, N., Sullivan, A. P., Skog, K., Keutsch, F. N., Collett, J. L., Jr., Decesari, S., Facchini, M.
515 C., Carlton, A. G., Laaksonen, A., and Turpin, B. J.: Aerosol liquid water driven by
516 anthropogenic nitrate: implications for lifetimes of water-soluble organic gases and potential for
517 secondary organic aerosol formation, *Environ. Sci. Technol.*, 48, 11127-11136,
518 doi:10.1021/es5025096, 2014.
- 519 Holmes, C. D., Bertram, T. H., Confer, K. L., Grahams, K. A., Ronan, A. C., Wirks, C. K., and
520 Shah, V.: The Role of Clouds in the Tropospheric NO_x Cycle: A New Modeling Approach for
521 Cloud Chemistry and Its Global Implications, *Geophys. Res. Lett.*, 46, 4980-4990,
522 doi:10.1029/2019gl081990, 2019.



-
- 523 Huang, D. D., Zhang, Q., Cheung, H. H. Y., Yu, L., Zhou, S., Anastasio, C., Smith, J. D., and
524 Chan, C. K.: Formation and Evolution of aqSOA from Aqueous-Phase Reactions of Phenolic
525 Carbonyls: Comparison between Ammonium Sulfate and Ammonium Nitrate Solutions,
526 *Environ. Sci. Technol.*, 52, 9215-9224, doi:10.1021/acs.est.8b03441, 2018.
- 527 Jeong, C. H., McGuire, M. L., Godri, K. J., Slowik, J. G., Rehbein, P. J. G., and Evans, G. J.:
528 Quantification of aerosol chemical composition using continuous single particle measurements,
529 *Atmos. Chem. Phys.*, 11, 7027-7044, doi:10.5194/acp-11-7027-2011, 2011.
- 530 Kaur, R., and Anastasio, C.: Light absorption and the photoformation of hydroxyl radical and
531 singlet oxygen in fog waters, *Atmos. Environ.*, 164, 387-397,
532 doi:10.1016/j.atmosenv.2017.06.006, 2017.
- 533 Leaitch, W. R., Bottenheim, J. W., and Strapp, J. W.: Possible contribution of N₂O₅ scavenging
534 to HNO₃ observed in winter stratiform cloud, *J. Geophys. Res.-Atmos.*, 93, 12569-12584,
535 doi:10.1029/JD093iD10p12569, 1988.
- 536 Li, H. Y., Zhang, Q., Zheng, B., Chen, C. R., Wu, N. N., Guo, H. Y., Zhang, Y. X., Zheng, Y. X.,
537 Li, X., and He, K. B.: Nitrate-driven urban haze pollution during summertime over the North
538 China Plain, *Atmos. Chem. Phys.*, 18, 5293-5306, doi:10.5194/acp-18-5293-2018, 2018.
- 539 Li, L., Huang, Z. X., Dong, J. G., Li, M., Gao, W., Nian, H. Q., Fu, Z., Zhang, G. H., Bi, X. H.,
540 Cheng, P., and Zhou, Z.: Real time bipolar time-of-flight mass spectrometer for analyzing single
541 aerosol particles, *Intl. J. Mass. Spectrom.*, 303, 118-124, doi:10.1016/j.ijms.2011.01.017, 2011.
- 542 Li, S., Zhang, F., Jin, X., Sun, Y., Wu, H., Xie, C., Chen, L., Liu, J., Wu, T., Jiang, S., Cribb, M.,
543 and Li, Z.: Characterizing the ratio of nitrate to sulfate in ambient fine particles of urban Beijing
544 during 2018–2019, *Atmos. Environ.*, 117662, doi:10.1016/j.atmosenv.2020.117662, 2020a.
- 545 Li, T., Wang, Z., Wang, Y. R., Wu, C., Liang, Y. H., Xia, M., Yu, C., Yun, H., Wang, W. H.,
546 Wang, Y., Guo, J., Herrmann, H., and Wang, T.: Chemical characteristics of cloud water and the
547 impacts on aerosol properties at a subtropical mountain site in Hong Kong SAR, *Atmos. Chem.*
548 *Phys.*, 20, 391-407, doi:10.5194/acp-20-391-2020, 2020b.
- 549 Lin, Q., Zhang, G., Peng, L., Bi, X., Wang, X., Brechtel, F. J., Li, M., Chen, D., Peng, P. a.,
550 Sheng, G., and Zhou, Z.: In situ chemical composition measurement of individual cloud residue
551 particles at a mountain site, southern China, *Atmos. Chem. Phys.*, 17, 8473-8488,



-
- 552 doi:10.5194/acp-17-8473-2017, 2017.
- 553 Lin, Y. C., Zhang, Y. L., Yu, M., Fan, M. Y., Xie, F., Zhang, W. Q., Wu, G., Cong, Z., and
554 Michalski, G.: Formation Mechanisms and Source Apportionments of Airborne Nitrate
555 Aerosols at a Himalayan-Tibetan Plateau Site: Insights from Nitrogen and Oxygen Isotopic
556 Compositions, *Environ. Sci. Technol.*, 55, 12261-12271, doi:10.1021/acs.est.1c03957, 2021.
- 557 Liu, H. Y., Crawford, J. H., Pierce, R. B., Norris, P., Platnick, S. E., Chen, G., Logan, J. A.,
558 Yantosca, R. M., Evans, M. J., Kittaka, C., Feng, Y., and Tie, X. X.: Radiative effect of clouds
559 on tropospheric chemistry in a global three-dimensional chemical transport model, *J. Geophys.*
560 *Res.-Atmos.*, 111, 18, doi:10.1029/2005jd006403, 2006.
- 561 Liu, L., Bei, N. F., Hu, B., Wu, J. R., Liu, S. X., Li, X., Wang, R. N., Liu, Z. R., Shen, Z. X.,
562 and Li, G. H.: Wintertime nitrate formation pathways in the north China plain: Importance of
563 N₂O₅ heterogeneous hydrolysis, *Environ. Pollut.*, 266, 10, doi:10.1016/j.envpol.2020.115287,
564 2020a.
- 565 Liu, P., Ye, C., Xue, C., Zhang, C., Mu, Y., and Sun, X.: Formation mechanisms of atmospheric
566 nitrate and sulfate during the winter haze pollution periods in Beijing: gas-phase, heterogeneous
567 and aqueous-phase chemistry, *Atmos. Chem. Phys.*, 20, 4153-4165, doi:10.5194/acp-20-4153-
568 2020, 2020b.
- 569 Lu, K., Fuchs, H., Hofzumahaus, A., Tan, Z., Wang, H., Zhang, L., Schmitt, S. H., Rohrer, F.,
570 Bohn, B., Broch, S., Dong, H., Gkatzelis, G. I., Hohaus, T., Holland, F., Li, X., Liu, Y., Liu, Y.,
571 Ma, X., Novelli, A., Schlag, P., Shao, M., Wu, Y., Wu, Z., Zeng, L., Hu, M., Kiendler-Scharr,
572 A., Wahner, A., and Zhang, Y.: Fast Photochemistry in Wintertime Haze: Consequences for
573 Pollution Mitigation Strategies, *Environ. Sci. Technol.*, 53, 10676-10684,
574 doi:10.1021/acs.est.9b02422, 2019.
- 575 McNeill, V. F.: Atmospheric Aerosols: Clouds, Chemistry, and Climate, *Annu. Rev. Chem.*
576 *Biomol.*, 8, 427-444, doi:10.1146/annurev-chembioeng-060816-101538, 2017.
- 577 Neuman, J. A., Nowak, J. B., Brock, C. A., Trainer, M., Fehsenfeld, F. C., Holloway, J. S.,
578 Hubler, G., Hudson, P. K., Murphy, D. M., Nicks, D. K., Orsini, D., Parrish, D. D., Ryerson, T.
579 B., Sueper, D. T., Sullivan, A., and Weber, R.: Variability in ammonium nitrate formation and
580 nitric acid depletion with altitude and location over California, *J. Geophys. Res.-Atmos.*, 108,



-
- 581 12, doi:10.1029/2003jd003616, 2003.
- 582 Pathak, R. K., Wu, W. S., and Wang, T.: Summertime PM_{2.5} ionic species in four major cities of
583 China: nitrate formation in an ammonia-deficient atmosphere, *Atmos. Chem. Phys.*, 9, 1711-
584 1722, 2009.
- 585 Prabhakar, G., Ervens, B., Wang, Z., Maudlin, L. C., Coggon, M. M., Jonsson, H. H., Seinfeld,
586 J. H., and Sorooshian, A.: Sources of nitrate in stratocumulus cloud water: Airborne
587 measurements during the 2011 E-PEACE and 2013 NiCE studies, *Atmos. Environ.*, 97, 166-
588 173, doi:10.1016/j.atmosenv.2014.08.019, 2014.
- 589 Pratt, K. A., DeMott, P. J., French, J. R., Wang, Z., Westphal, D. L., Heymsfield, A. J., Twohy,
590 C. H., Prenni, A. J., and Prather, K. A.: In situ detection of biological particles in cloud ice-
591 crystals, *Nature Geosci.*, 2, 397-400, 2009.
- 592 Qu, K., Wang, X., Xiao, T., Shen, J., Lin, T., Chen, D., He, L.-Y., Huang, X.-F., Zeng, L., Lu,
593 K., Ou, Y., and Zhang, Y.: Cross-regional transport of PM_{2.5} nitrate in the Pearl River Delta,
594 China: Contributions and mechanisms, *Sci. Total. Environ.*, 753,
595 doi:10.1016/j.scitotenv.2020.142439, 2021.
- 596 Riemer, N., Vogel, H., Vogel, B., Schell, B., Ackermann, I., Kessler, C., and Hass, H.: Impact
597 of the heterogeneous hydrolysis of N₂O₅ on chemistry and nitrate aerosol formation in the lower
598 troposphere under photochemical conditions, *J. Geophys. Res.-Atmos.*, 108, 21,
599 doi:10.1029/2002jd002436, 2003.
- 600 Roth, A., Schneider, J., Klimach, T., Mertes, S., van Pinxteren, D., Herrmann, H., and Borrmann,
601 S.: Aerosol properties, source identification, and cloud processing in orographic clouds
602 measured by single particle mass spectrometry on a central European mountain site during
603 HCCT-2010, *Atmos. Chem. Phys.*, 16, 505-524, doi:10.5194/acp-16-505-2016, 2016.
- 604 Scharko, N. K., Berke, A. E., and Raff, J. D.: Release of Nitrous Acid and Nitrogen Dioxide
605 from Nitrate Photolysis in Acidic Aqueous Solutions, *Environ. Sci. Technol.*, 48, 11991-12001,
606 doi:10.1021/es503088x, 2014.
- 607 Schneider, J., Mertes, S., van Pinxteren, D., Herrmann, H., and Borrmann, S.: Uptake of nitric
608 acid, ammonia, and organics in orographic clouds: mass spectrometric analyses of droplet
609 residual and interstitial aerosol particles, *Atmos. Chem. Phys.*, 17, 1571-1593, doi:10.5194/acp-



-
- 610 17-1571-2017, 2017.
- 611 Seinfeld, J. H., and Pandis, S. N.: Atmospheric Chemistry and Physics: From Air Pollution to
612 Climate Change, edited by: John Wiley&Sons, I., John Wiley&Sons, Inc., New Jersey, 2006.
- 613 Sellegri, K., Laj, P., Marinoni, A., Dupuy, R., Legrand, M., and Preunkert, S.: Contribution of
614 gaseous and particulate species to droplet solute composition at the Puy de Dome, France,
615 Atmos. Chem. Phys., 3, 1509-1522, doi:10.5194/acp-3-1509-2003, 2003.
- 616 Shi, X., Nenes, A., Xiao, Z., Song, S., Yu, H., Shi, G., Zhao, Q., Chen, K., Feng, Y., and Russell,
617 A. G.: High-Resolution Data Sets Unravel the Effects of Sources and Meteorological Conditions
618 on Nitrate and Its Gas-Particle Partitioning, Environ. Sci. Technol., 53, 3048-3057,
619 doi:10.1021/acs.est.8b06524, 2019.
- 620 Shingler, T., Dey, S., Sorooshian, A., Brechtel, F. J., Wang, Z., Metcalf, A., Coggon, M.,
621 Mulmenstadt, J., Russell, L. M., Jonsson, H. H., and Seinfeld, J. H.: Characterisation and
622 airborne deployment of a new counterflow virtual impactor inlet, Atmos. Meas. Tech., 5, 1259-
623 1269, doi:10.5194/amt-5-1259-2012, 2012.
- 624 Song, X. H., Hopke, P. K., Fergenson, D. P., and Prather, K. A.: Classification of single particles
625 analyzed by ATOFMS using an artificial neural network, ART-2A, Anal. Chem., 71, 860-865,
626 1999.
- 627 Strode, S. A., Douglass, A. R., Ziemke, J. R., Manyin, M., Nielsen, J. E., and Oman, L. D.: A
628 Model and Satellite-Based Analysis of the Tropospheric Ozone Distribution in Clear Versus
629 Convectively Cloudy Conditions, J. Geophys. Res.-Atmos., 122, 11948-11960,
630 doi:10.1002/2017jd027015, 2017.
- 631 Sultana, C. M., Cornwell, G. C., Rodriguez, P., and Prather, K. A.: FATES: a flexible analysis
632 toolkit for the exploration of single-particle mass spectrometer data, Atmos. Meas. Tech., 10,
633 1323-1334, doi:10.5194/amt-10-1323-2017, 2017.
- 634 Sun, J. X., Liu, L., Xu, L., Wang, Y. Y., Wu, Z. J., Hu, M., Shi, Z. B., Li, Y. J., Zhang, X. Y.,
635 Chen, J. M., and Li, W. J.: Key Role of Nitrate in Phase Transitions of Urban Particles:
636 Implications of Important Reactive Surfaces for Secondary Aerosol Formation, J. Geophys.
637 Res.-Atmos., 123, 1234-1243, doi:10.1002/2017JD027264, 2018.
- 638 Tao, J., Zhang, Z., Tan, H., Zhang, L., Wu, Y., Sun, J., Che, H., Cao, J., Cheng, P., Chen, L., and



-
- 639 Zhang, R.: Observational evidence of cloud processes contributing to daytime elevated nitrate
640 in an urban atmosphere, *Atmos. Environ.*, 186, 209-215, doi:10.1016/j.atmosenv.2018.05.040,
641 2018.
- 642 Tian, M., Liu, Y., Yang, F. M., Zhang, L. M., Peng, C., Chen, Y., Shi, G. M., Wang, H. B., Luo,
643 B., Jiang, C. T., Li, B., Takeda, N., and Koizumi, K.: Increasing importance of nitrate formation
644 for heavy aerosol pollution in two megacities in Sichuan Basin, southwest China, *Environ.*
645 *Pollut.*, 250, 898-905, doi:10.1016/j.envpol.2019.04.098, 2019.
- 646 Voulgarakis, A., Wild, O., Savage, N. H., Carver, G. D., and Pyle, J. A.: Clouds, photolysis and
647 regional tropospheric ozone budgets, *Atmos. Chem. Phys.*, 9, 8235-8246, doi:10.5194/acp-9-
648 8235-2009, 2009.
- 649 Wang, H., Lu, K., Chen, X., Zhu, Q., Chen, Q., Guo, S., Jiang, M., Li, X., Shang, D., Tan, Z.,
650 Wu, Y., Wu, Z., Zou, Q., Zheng, Y., Zeng, L., Zhu, T., Hu, M., and Zhang, Y.: High N₂O₅
651 Concentrations Observed in Urban Beijing: Implications of a Large Nitrate Formation Pathway,
652 *Environ. Sci. Tech. Let.*, doi:10.1021/acs.estlett.7b00341, 2017.
- 653 Wang, X. F., Zhang, Y. P., Chen, H., Yang, X., Chen, J. M., and Geng, F. H.: Particulate Nitrate
654 Formation in a Highly Polluted Urban Area: A Case Study by Single-Particle Mass
655 Spectrometry in Shanghai, *Environ. Sci. Technol.*, 43, 3061-3066, doi:10.1021/es8020155,
656 2009.
- 657 Wen, L., Xue, L. K., Wang, X. F., Xu, C. H., Chen, T. S., Yang, L. X., Wang, T., Zhang, Q. Z.,
658 and Wang, W. X.: Summertime fine particulate nitrate pollution in the North China Plain:
659 increasing trends, formation mechanisms and implications for control policy, *Atmos. Chem.*
660 *Phys.*, 18, 11261-11275, doi:10.5194/acp-18-11261-2018, 2018.
- 661 Wu, C., Liu, L., Wang, G., Zhang, S., Li, G., Lv, S., Li, J., Wang, F., Meng, J., and Zens, Y.:
662 Important contribution of N₂O₅ hydrolysis to the daytime nitrate in Xi'an, China during haze
663 periods: Isotopic analysis and WRF-Chem model simulation, *Environ. Pollut.*, 117712,
664 doi:10.1016/j.envpol.2021.117712, 2021.
- 665 Xiao, H.-W., Zhu, R.-G., Pan, Y.-Y., Guo, W., Zheng, N.-J., Liu, Y.-H., Liu, C., Zhang, Z.-Y.,
666 Wu, J.-F., Kang, C.-A., Luo, L., and Xiao, H.-Y.: Differentiation Between Nitrate Aerosol
667 Formation Pathways in a Southeast Chinese City by Dual Isotope and Modeling Studies, *J.*



-
- 668 Geophys. Res.-Atmos., 125, doi:10.1029/2020jd032604, 2020.
- 669 Xu, L., and Penner, J. E.: Global simulations of nitrate and ammonium aerosols and their
670 radiative effects, *Atmos. Chem. Phys.*, 12, 9479-9504, doi:10.5194/acp-12-9479-2012, 2012.
- 671 Xu, Q., Wang, S., Jiang, J., Bhattarai, N., Li, X., Chang, X., Qiu, X., Zheng, M., Hua, Y., and
672 Hao, J.: Nitrate dominates the chemical composition of PM_{2.5} during haze event in Beijing,
673 China, *Sci. Total. Environ.*, 689, 1293-1303, doi:10.1016/j.scitotenv.2019.06.294, 2019.
- 674 Yan, C., Tham, Y. J., Zha, Q. Z., Wang, X. F., Xue, L. K., Dai, J. N., Wang, Z., and Wang, T.:
675 Fast heterogeneous loss of N₂O₅ leads to significant nighttime NO_x removal and nitrate aerosol
676 formation at a coastal background environment of southern China, *Sci. Total. Environ.*, 677,
677 637-647, doi:10.1016/j.scitotenv.2019.04.389, 2019.
- 678 Ye, C., Heard, D. E., and Whalley, L. K.: Evaluation of Novel Routes for NO_x Formation in
679 Remote Regions, *Environ. Sci. Technol.*, 51, 7442-7449, doi:10.1021/acs.est.6b06441, 2017a.
- 680 Ye, C., Zhang, N., Gao, H., and Zhou, X.: Photolysis of Particulate Nitrate as a Source of HONO
681 and NO_x, *Environ. Sci. Technol.*, 51, 6849-6856, doi:10.1021/acs.est.7b00387, 2017b.
- 682 Zhai, S., Jacob, D. J., Wang, X., Liu, Z., Wen, T., Shah, V., Li, K., Moch, J. M., Bates, K. H.,
683 Song, S., Shen, L., Zhang, Y., Luo, G., Yu, F., Sun, Y., Wang, L., Qi, M., Tao, J., Gui, K., Xu,
684 H., Zhang, Q., Zhao, T., Wang, Y., Lee, H. C., Choi, H., and Liao, H.: Control of particulate
685 nitrate air pollution in China, *Nature Geosci.*, 14, 389-395, doi:10.1038/s41561-021-00726-z,
686 2021.
- 687 Zhang, G. H., Lin, Q. H., Peng, L., Yang, Y. X., Fu, Y. Z., Bi, X. H., Li, M., Chen, D. H., Chen,
688 J. X., Cai, Z., Wang, X. M., Peng, P. A., Sheng, G. Y., and Zhou, Z.: Insight into the in-cloud
689 formation of oxalate based on in situ measurement by single particle mass spectrometry, *Atmos.*
690 *Chem. Phys.*, 17, 13891-13901, doi:10.5194/acp-17-13891-2017, 2017.
- 691 Zhang, J., Lance, S., Brandt, R., Marto, J., Ninneman, M., and Schwab, J.: Observed below-
692 Cloud and Cloud Interstitial Submicron Aerosol Chemical and Physical Properties at Whiteface
693 Mountain, New York, during August 2017, *Acs Earth Space Chem.*, 3, 1438-1450,
694 doi:10.1021/acsearthspacechem.9b00117, 2019.
- 695 Zhang, R., Gen, M., Fu, T. M., and Chan, C. K.: Production of Formate via Oxidation of Glyoxal
696 Promoted by Particulate Nitrate Photolysis, *Environ. Sci. Technol.*, 55, 5711-5720,



697 doi:10.1021/acs.est.0c08199, 2021.
698 Zheng, H., Song, S., Sarwar, G., Gen, M., Wang, S., Ding, D., Chang, X., Zhang, S., Xing, J.,
699 Sun, Y., Ji, D., Chan, C. K., Gao, J., and McElroy, M. B.: Contribution of Particulate Nitrate
700 Photolysis to Heterogeneous Sulfate Formation for Winter Haze in China, Environ. Sci. Tech.
701 Let., 7, 632-638, doi:10.1021/acs.estlett.0c00368, 2020.
702 Zhu, Y., Tilgner, A., Hoffmann, E. H., Herrmann, H., Kawamura, K., Yang, L., Xue, L., and
703 Wang, W.: Multiphase MCM-CAPRAM modeling of the formation and processing of secondary
704 aerosol constituents observed during the Mt. Tai summer campaign in 2014, Atmos. Chem.
705 Phys., 20, 6725-6747, doi:10.5194/acp-20-6725-2020, 2020.
706



707 **Figure captions:**

708 **Figure 1.** Box-and-whisker plots of (a) the mass fraction of nitrate in PM_{2.5} and cloud
709 water and (b) the RPA of nitrate separated for the cloud-free, cloud residual (RES),
710 and cloud interstitial (INT) particles, in 2018 spring and 2020 winter, respectively. In
711 a box and whisker plot, the lower, median and upper line of the box denotes the 25,
712 50, and 75 percentiles, respectively; the lower and upper edges of the whisker denote
713 the 10 and 90 percentiles, respectively.

714 **Figure 2.** Size dependent RPA of nitrate and RPA ratio of nitrate/sulfate, separated
715 for all the detected cloud-free, cloud residual (RES), and cloud interstitial (INT)
716 particles, in (a) 2018 spring (May) and (b) 2020 winter (Nov-Dec), respectively.

717 **Figure 3.** Theoretical calculation of the trend of in-cloud produced nitrate from the
718 hydrolysis of N₂O₅ versus the temporal variations of NO₃ concentration in cloud
719 water in 2020 winter (Nov-Dec).

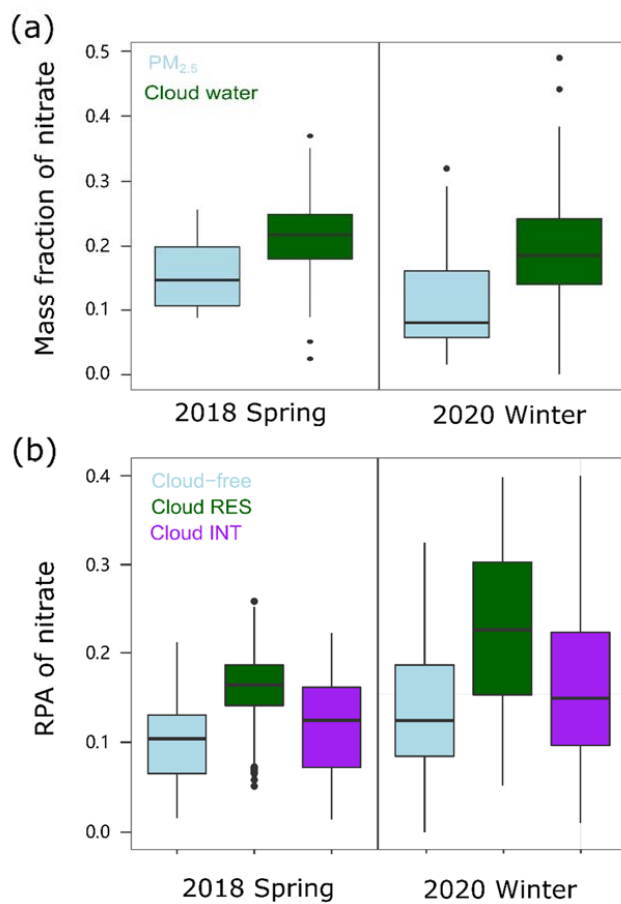
720 **Figure 4.** Correlation analysis between the observed RPAs of nitrate and the
721 predicted RPAs of nitrate, with inputs of NO₂, O₃ and LWC, for the (a) cloud-free and
722 (b) cloud RES particles, respectively.

723 **Figure 5.** Relative contribution of each pathway to the nitrate production in wet
724 aerosols (WA, 0.5 μm) and cloud droplets (CD, 8 μm), respectively, simulated by the
725 RACM-CAPRAM. The atmospheric conditions considered for comparison are LWC



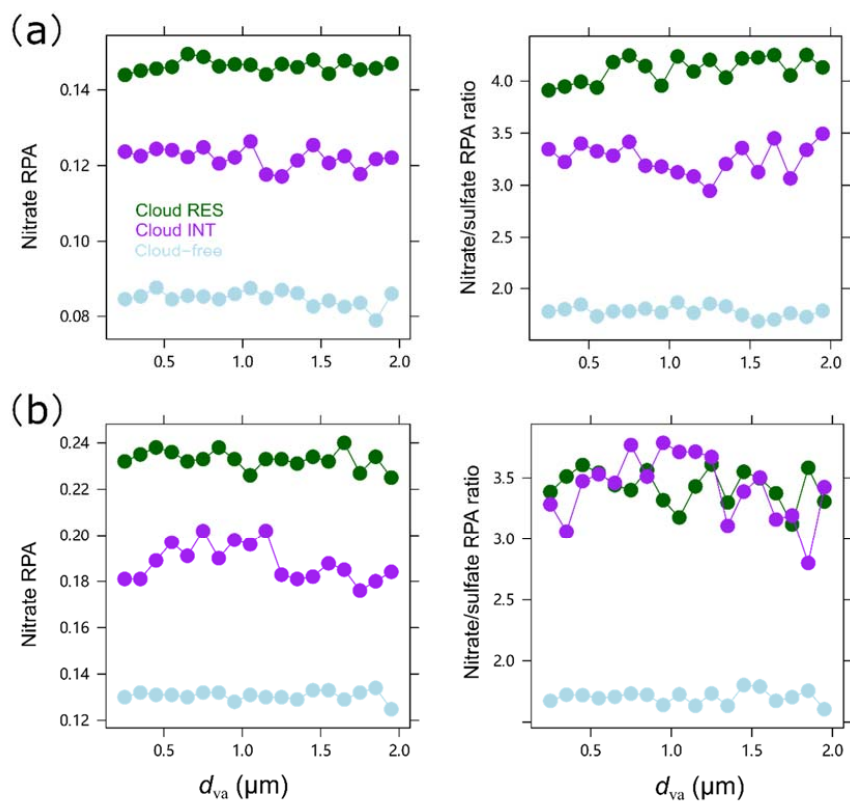
726 $(10^{-5}$ - 10^{-4} g cm⁻³ for wet aerosols and 0.05-0.15 g cm⁻³) and photolysis rates (30%,

727 50%, 100%).



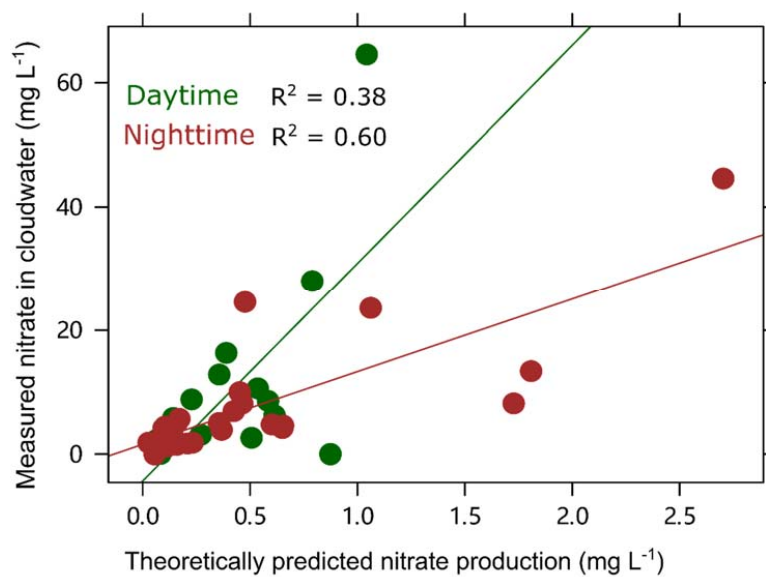
728

729 **Fig. 1.**



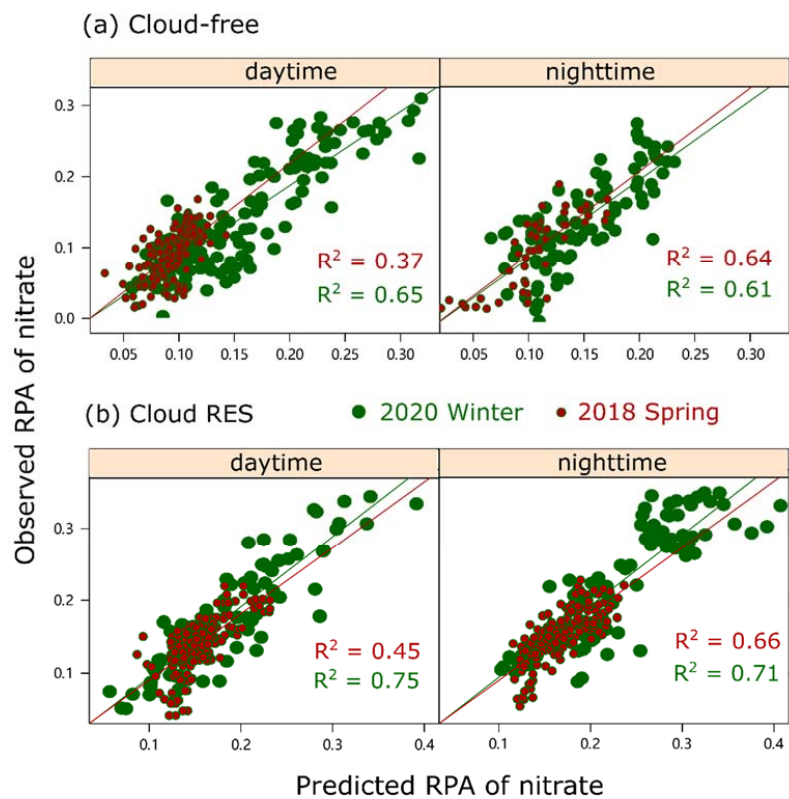
730

731 **Fig. 2.**



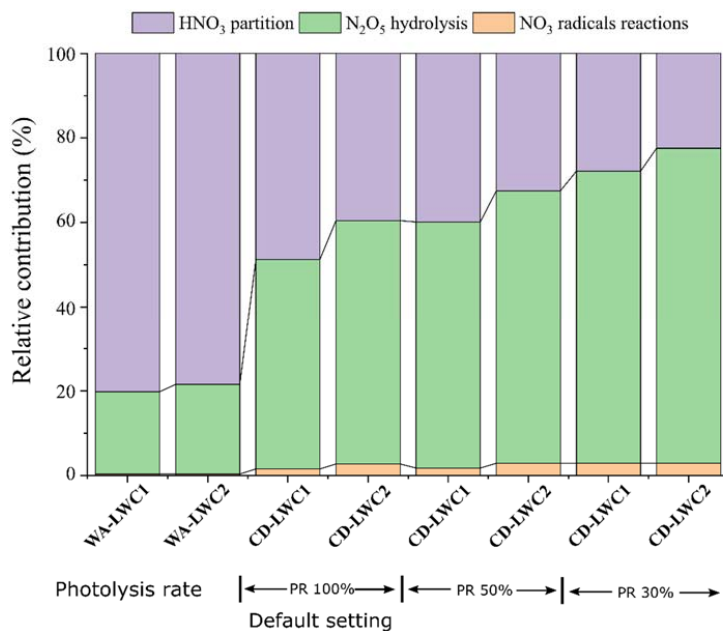
732

733 **Fig. 3.**



734

735 **Fig. 4.**



736

737 **Fig. 5.**